Characterize Planetary Surfaces from a Single Point to a Large Area Using a Standoff Ultra-Compact µ-Raman Instrument

M. NURUL ABEDIN[1], ARTHUR T. BRADLEY[1], ANUPAM K. MISRA[2], ALAN D. LITTLE[1], GLENN D. HINES[1], BRUCE BARNES[1], YINGXIN BAI[3], CHRISTOPHER P. MCKAY[4], PAUL G. LUCEY[2], AND ANDREW STEELE[5]

[1]*NASA Langley Research Center, Hampton, VA 23681*
[2]*University of Hawaii at Manoa, Honolulu, Hawaii 96822*
[3]*NASA Goddard Space Flight Center, Greenbelt, MD 20771*
[4]*NASA Ames Research Center, Moffett Field, CA 94035*
[5]*Carnegie Institution of Washington, Washington-DC, DC 20015*
*Corresponding Author: m.n.abedin@nasa.gov

Abstract

A standoff Ultra-Compact micro-Raman (SUCR) instrument is used for detection of minerals, organic, and biological materials in daylight and nighttime conditions. The standoff measurements from a SUCR instrument based on micro-Raman spectroscopy on a rover or lander platform is ideal for identifying various types of ices, minerals, organics and biogenic materials. The µ-Raman measurements can assist in determining the biological potential for habitability assessment of planetary bodies as well as amino acid detection for evidence of past or present life on Mars, Europa, and other solar bodies. The SUCR instrument is used to inspect minerals, organic, biomarkers, ice, and embedded materials inside ice, as well as to conduct Raman line scanning from a single point to a large area for standoff detection at a 6-cm target distance.

----

1. INTRODUCTION

The discovery of life in our Solar System beyond that on Earth is an important goal outlined in the NASA Decadal Survey 2013-2022.[1] The detection of biological materials and biomarkers would be evidence in support of life outside our planet and is an important step towards meeting the goals of the NASA Planetary Exploration Program. Raman spectroscopy has been identified as suitable for detection of "Search for life" elements. Two traditional micro-Raman systems were identified in the Europa Lander Study 2016 Report: 1) "SHERLOC", a Deep UV micro-Raman system operating at 248.6 nm continuous wave (CW) laser for Mars 2020 and 2) "Raman Laser Spectrometer (RLS)", a micro-Raman system operating at 532 nm CW laser for ExoMars.[2] In addition, as discussed in our previous SUCR paper[3], a standoff µ-Raman instrument was developed at NASA Langley Research Center (LaRC) using a 532 nm pulsed time gated Raman technology. Raman spectroscopy uses an active laser interrogation with targets. The primary advantage of Raman spectroscopy over passive spectroscopy is the sharpness of spectral features for minerals, which results in significantly less ambiguity in the detection of specific species, especially the presence of mineral mixtures. We prepared a few different complex samples in the NASA LaRC

Laboratory and these are: (1) a thin layer of glutamine (amino acid) was deposited on bulk calcite substrate and another thin layer of soil was deposited on top of the glutamine layer to make a complex three-layered sample. (2) A second complex sample with the mixture of sand, naphthalene, and sulfur; and (3) a third mixed sample with soil, glutamine, naphthalene, and sulfur. We characterized bulk calcite, hydrous minerals (e.g., bulk Gypsum, Alabaster, and Alabaster in ice) and amino acids (bulk L-Glutamine and Glutamine in ice), as well as the above-mentioned complex samples by utilizing a Micro-Raman sensor. We collected Raman signals from hydrous minerals, amino acids, and mixed samples and analyzed them using a GRAMS/AI software. This characterization demonstrates and confirms the SUCR sensor's capabilities of hydrous minerals, biomarkers, and mixed samples (mixed calcite/glutamine/soil and sand/gypsum in ice) that might be embedded in the Mars and Lunar soil, sand, and ice within a single Raman measurement allowing for faster Raman detection and identification.

For micro-Raman imaging, Privitera et al. (2001) performed micro-Raman measurements on a Silicide sample using a Labram (Dilor) confocal spectrometer and a 17 mW HeNe laser with a laser spot 0.7 µm in diameter. The spectra were recorded by scanning the sample surface with an increment of 0.5 µm step and 20,000 spectra were obtained over a silicide (100 x 50 μm^2) area with an integration time of 4s.[4] Dall'Asén et al. (2017) published a paper on the use of a confocal micro-Raman system (WITec, Alpha300) on composite Raman line scan images taken with low- and high-resolution gratings along a linear path across the large chondrule (chondritic meteorite Northwest Africa 3118).[5] The scan lines were obtained across the studied region (~3 µm x 3.3 mm), where a laser (488 nm Ar^+) spot diameter was ~3 µm and its power was ~ 5 mw on the sample.[5] Beegle et al. (2016) demonstrated the mapping of organic molecules over a carbonate sample and the ability of Scanning Habitable Environments with Raman & Luminescence for Organics and Chemicals (SHERLOC) to identify potential biosignatures.[6] A map of the fluorescent features identified organic structure that was not visible. A Raman spectrum was obtained from the invisible region within the fluorescent mapping area that showed spectral features of organic materials.[6]

In this paper, we discuss SUCR instrument design and fabrication and measurement capabilities from a Raman single point to a large line scanning.

2. SUCR INSTRUMENT DESIGN AND OPERATION

Fig.1 shows the SUCR instrument optical design in Fig. 1(a), 3-D enclosure in Fig. 1(b), holographic grating, c-mount lenses inside spectrograph in Fig. 1(c), and mounting optical components, an intensified charge-coupled device (ICCD), laser and a neon light is shown in Fig. 1(d), but the neon light source was far away from the collecting optics in the picture. The target distance of 6 cm from the collecting optics was used to achieve the minimum laser spot size 10 µm x 5 mm, which is determined through an optical ray design using the 532-nm laser with 0.2-mJ energy at 1-kHz repetition rate (see Fig. 1(a, d)).

The 532 nm excitation laser generates a beam that is reflected 45° using a mirror and then pointed towards the target material using a dichroic mirror notch filter. The notch filter is specially coated to reflect 532 nm signals while passing all other wavelengths. Once the beam has reflected back into the system, notch filter 1 (45º) and notch filter 2 (0º) will filter out the remaining 532 nm signal to ensure that none of the incident light passes into the spectrometer.

Once only, a 50 mm C-mount lens collects the Raman signal remains it. This lens focuses the signal through the 50-micron entrance slit and into the spectrometer. After the slit, the signal is then collimated using another 50 mm C-mount lens and passed through a holographic transmission grating where the varying

wavelengths are separated into a spectrum and transmitted out at 45°. The transmitted spectrum is then passed through a final 50 mm C-mount lens to be focused before being passed into the ICCD camera. The ICCD will capture the spectral image and convert it into spectrum for processing on a terminal.
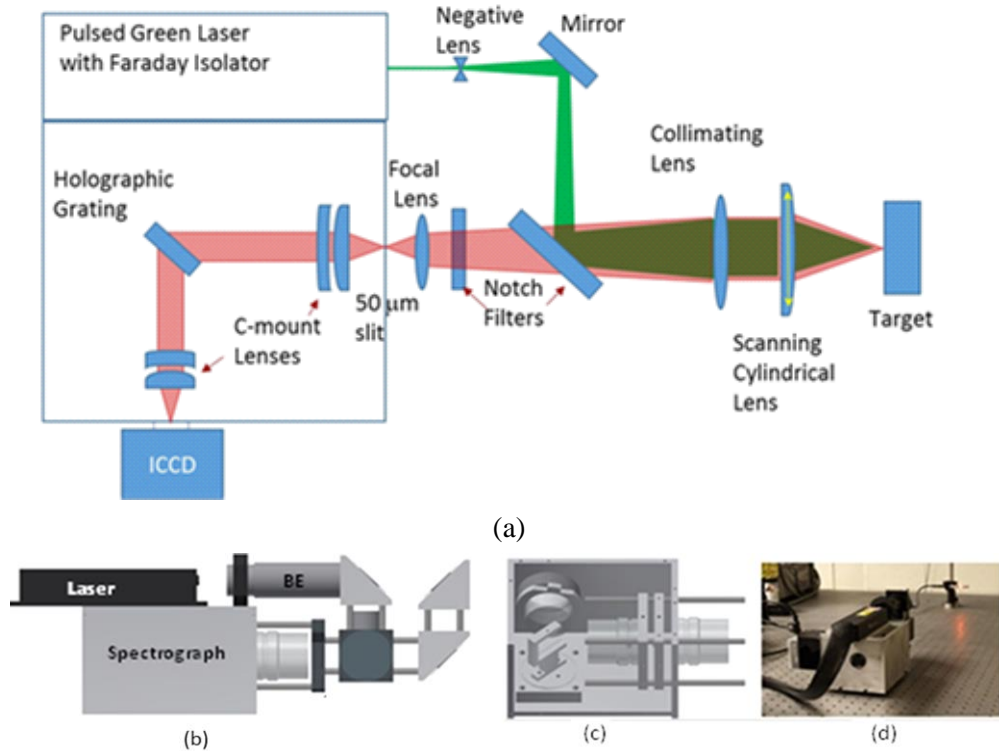

(a)

(b) (c) (d)

Fig. 1. SUCR instrument: a. Optical Design, b. 3-D enclosure, c. spectrograph, and d. prototype SUCR instrument.

3. STANDOFF -RAMAN SYSTEM MEASUREMENT CAPABILITIES

Fig. 2. SUCR Sensor with an ICCD camera, laser, spectrograph, collecting optics and a target sample.

We built an ultracompact -Raman system using direct coupling between the compact spectrograph and the one-inch collecting optics for high throughput efficiency. This spectrometer was built in-house using procured optical components from Kaiser custom-built grating, C-mount lenses from Thorlabs, notch filters from Semrock, and other optics from Edmund Optics.

We integrated the SUCR instrument using a 532 nm pulsed laser with 0.2 mJ/pulse and 1 kHz repetition from CrystaLaser, LLC, an Intensified Charge-Coupled Device (ICCD) from Syntronics, Inc, and a spectrograph built at NASA LaRC. The target distance from the collecting optics is ~6 cm, which was determined through an optical design in Fig. 1a for a 60-mm cylindrical lens for generating a line-shaped laser excitation on the target. The SUCR system is designed for use on a rover/lander platform and interpret them in real time.

The system operates during both day and night conditions and, due to the pulsed gated Raman technology which significantly reduces the daylight background, is not restricted by background illumination and mineral

luminescence.[7] The mini-ICCD consumes 3.5 W with Peltier cooling. For a 6-cm target range, the total data collection time to collect a Raman line image ~10-micron width by 5 mm height is 0.1 second. The commercially available compact Q-Switch pulsed laser from Crystalaser operates at 0.20 mJ/pulse, 1 kHz, weighs 600 g, and consumes 40 W. The total energy consumption of the instrument is low because of the fast data collection.

The miniaturized spectrograph is based on a custom HoloPlex grating from KOSI and covers the entire Raman spectral range of 80 cm^{-1} to 4500 cm^{-1} (534.3 - 699.5 nm), Stokes-Raman shifted from the 532 nm laser excitation line. The mass of the system with the optics and laser is 4.6 kg. We demonstrated standoff spectra of sulfur, naphthalene, mixed naphthalene and sulfur, alabaster, and amino acids as mixed solid powders and also embedded inside ice using the above-mentioned spectrometer at a distance of 6 cm (a line shaped laser with 10 µm width by 5 mm height) as shown in Figs. 3 to 8. Furthermore, we mounted samples to be scanned on the surface of the Micos VT-80 Linear Stage (Motor) and then mapped 5 mm x 5 mm with a laser spot size 10-µm width by 5 mm height. The results of these mappings are discussed in Fig. 9.

4. RESULTS AND DISCUSSION

Fig. 3 depicts the low and high frequency regions in the Raman spectra of water and ice obtained with the SUCR system. This Raman instrument system has been demonstrated to have an excellent ability to measure the symmetric and antisymmetric stretching O-H vibrational modes of water molecules that can be found in the 3100-3600 cm^{-1} region of their Raman spectra, as can be seen in Fig. 3 in the spectra of water and ice.[8-11] In the measured Raman spectrum of ice, the location of the band is in the same region as that of liquid water, but it is distinctively characterized by a very sharp peak at 3174 cm^{-1}. The formation of stronger hydrogen bonds in ice causes the decrease in frequency of the symmetric O-H stretching mode of water

molecules. Therefore, detection of Raman bands in this region does not only indicate the presence of water, but the shape of the spectrum can also be analyzed to distinguish between liquid water and ice.

Fig. 4 shows the Raman spectra of sulfur, naphthalene, and mixed sulfur and naphthalene in dry (Fig. 4a) and embedded inside ice (Fig. 4b), respectively. Identifiable Raman lines were observed in both naphthalene and sulfur spectra. The Raman spectra of sulfur in Fig. 4 (green) are measured. The sharp and narrow Raman fingerprints are detected at 151, 219, 438, and 472 cm^{-1} for the low frequency region.[3]
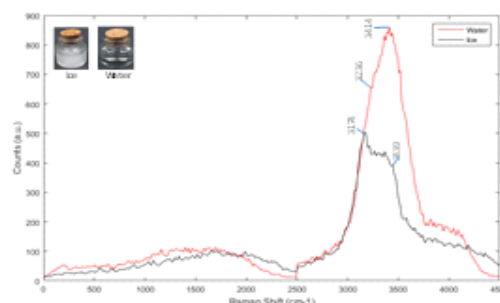

Fig. 3. Low and high frequency Raman spectra of liquid water (red) and ice (black) at 6-cm target distance.

At room and ice temperatures, crystalline sulfur exists as cyclic crown shaped S8 molecules.[12] There are eleven fundamental vibrational modes, and all of them are Raman active[12]. Three of the eleven fundamental modes give rise to intense, sharp Raman peaks (Fig. 4) at 151, 219, 438, and 472 cm^{-1}. These peaks are attributed to the doubly degenerate bending ($\nu8$), symmetric bending ($\nu2$), and symmetric stretching ($\nu1$) vibrations of the cyclic molecule, respectively.[12]

The Raman spectra of naphthalene, a Polycyclic Aromatic Hydrocarbon (PAH), sulfur, and mixed naphthalene and sulfur in dry in Fig. 4 (a); and ice and mixed naphthalene and sulfur embedded inside ice in Fig. 4 (b) are measured. The characteristic peaks are 123, 514, 764, 1021, 1146, 1380, 1464, 1575, and 1628 for the low frequency and 3064 (or 3065) cm^{-1} for

the high frequency regions (Figs. 4a (black) and 4b (red)).[7,13] The Raman peak at 3174 cm^{-1} and band 3174 - 3502 cm^{-1} are due to ice in Fig. 4b (red and black traces). Results in Fig. 4a (black) are compared with the results obtained by combining individual Raman spectra of naphthalene and sulfur at low and high frequency regions (Figs. 4a (red) and 4a (green)), which match very well with Fig. 4a (black) and Raman

spectra of mixed naphthalene, sulfur and ice in Fig. 4b (red). These data show that the SUCR system can detect sulfur, naphthalene, mixed naphthalene/sulfur embedded them inside ice, as well as ice band (Fig. 4b (red)). The standoff Raman measurements show that it is possible to detect sulfur, PAH, mixed PAH/sulfur, and ice-water band on the icy surface and subsurface of planetary bodies.
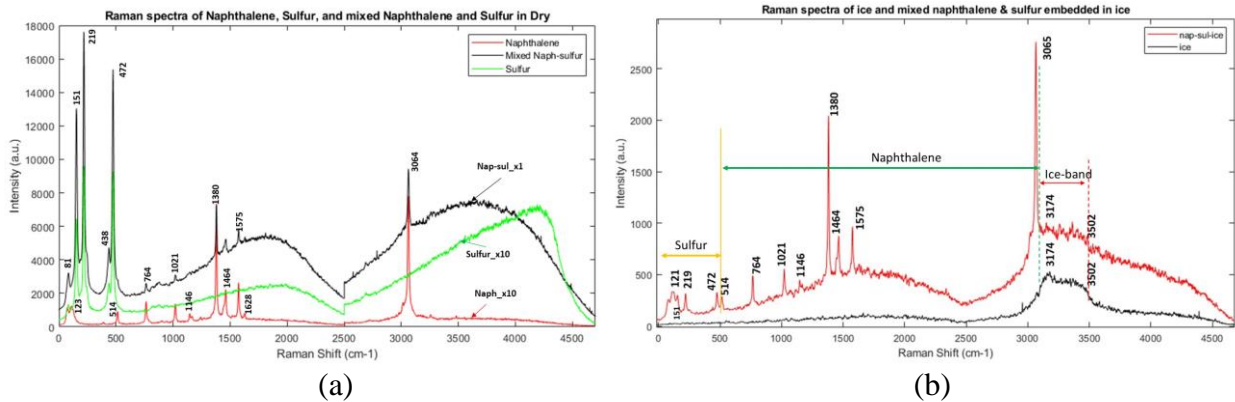

Fig. 4. Raman spectra of naphthalene, mixed naphthalene & sulfur, and sulfur in dry (red, black, and green) (a); and ice and mixed naphthalene& sulfur embedded in ice (black and red) (b) at low frequency and high frequency regions at a 6 cm target distance. 532 nm laser with energy 20 µJoule/pulse and 1 kHz repetition rate.

Fig. 5 shows the Raman spectra of Alabaster in dry and inside ice. Alabaster ($CaSO_4.2H_2O$) is massive fine-grained variety of gypsum and has similar chemistry as Gypsum. In this Fig. 5, we show the ability of the SUCR Raman system to detect hydrated sulfate mineral $CaSO_4.2H_2O$ in frequency region 100 to 4500 cm^{-1}, from a distance of 6-cm. The fingerprint Raman bands of this mineral are marked on the spectra. The symmetrical stretching mode of sulfate ions in $CaSO_4.2H_2O$ is observed at 1009 cm^{-1}, respectively. Very strong bands near 3100–3500 cm^{-1} in the Raman spectra of hydrous minerals indicate the O-H stretching modes of a chemically bonded water molecule. The

chemically bonded water molecules in alabaster are observed at 3410 cm^{-1} and 3496 cm^{-1} as shown in Fig. 5(a). The Raman spectra of mineral alabaster outside/inside ice are shown in the low and high frequency regions in Fig. 5. The low and high frequency spectra show a few sharp peaks at around 1007, 1134 cm^{-1} (low) and 3410, 3496 cm^{-1} (high) in Fig. 5 (a).[7,13,14] and 1007, 1134 cm^{-1} (low frequency region); and 3174, 3415, and 3502 cm-1 (high frequency region) in Fig. 5b. An extra peak was detected at 3174 cm^{-1}, which is due to an ice sharp peak. These experiments show that the standoff SUCR instrument can detect and identify various minerals frozen inside ice, providing for in-situ analysis on the icy surface of any planetary bodies.
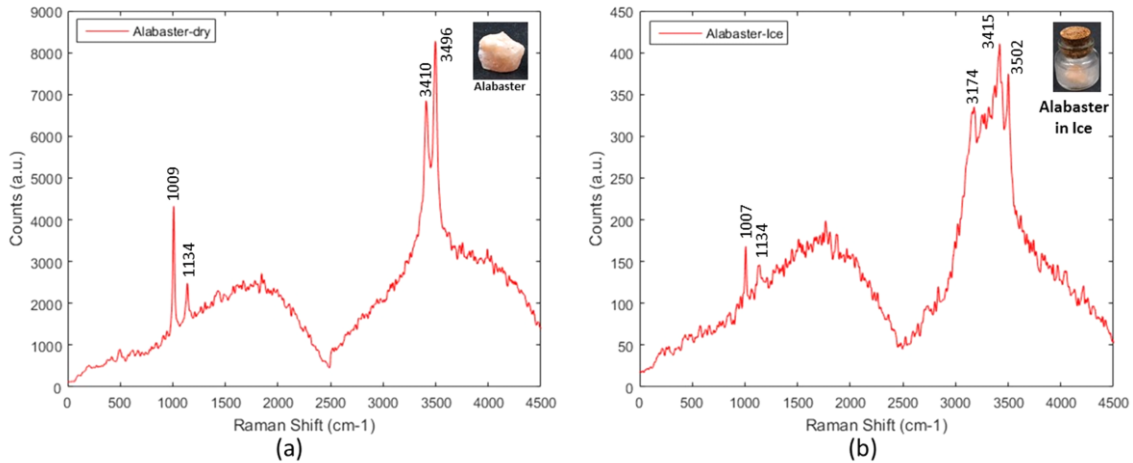
Fig. 5. Raman spectra of mineral alabaster in dry (a) and alabaster embedded inside ice (b).

In Figure 6, the Raman spectra of sulfate minerals gypsum (CaSO4·2H20) and alabaster are shown in both the low frequency range (Fig. 5a) and the high frequency range (Fig. 5b). All the spectra in the low frequency range in Figure 6a show the strong band at about 1006 cm^{-1}. In addition, the weak bands at around 418, 492, and 1136 cm^{-1} can be easily identified in the spectrum of gypsum sample. The observed bands are very much comparable to the reported Raman modes for gypsum at 418, 492, 1006, and 1136 cm^{-1}.[15-16] In the high frequency spectra shown in Figure 6b, two sharp bands at around 3407 and 3485 cm^{-1} are observed. These are due to the stretching modes of water molecules, which indicate the presence of chemically bonded two types of water molecules in an ordered structure.[17-18] In addition, the mixed sand/gypsum in ice are also shown in Fig. 6(a) and 6(b) as complex samples, respectively. It was possible to detect Atlantic ocean sand as broadband and gypsum in ice. The overall signal amplitude increases due to sand. This kind of mixed sample will be observed in the Mars or lunar surface.
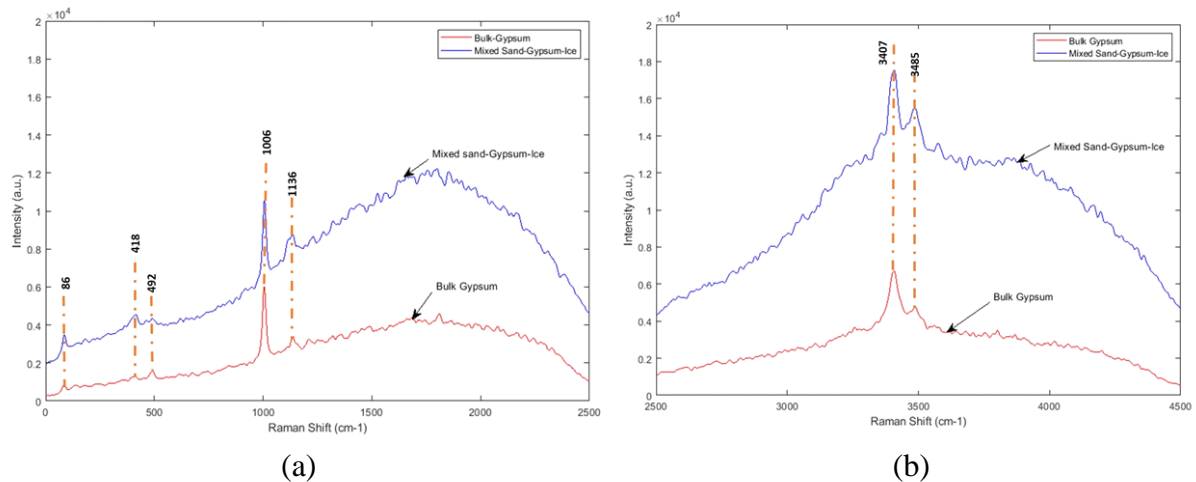

Fig. 6 Raman spectra of bulk gypsum and mixed gypsum/sand in dry (a) and bulk gypsum and mixed gypsum/sand in ice (b) at low and high frequency regions.

Fig. 7 shows the Raman spectra from biological materials (alanine, glutamine, and phenylalanine) after polynomial baseline correction at a 6-cm target distance. The Raman sharp peaks of alanine, glutamine, and phenylalanine are designated by employing Raman sharp peaks published in references.[20-24] The molecular structure of alanine is $C_3H_7NO_2$ and peaks are detected at 112 (H_2C-CH_2), 284, 526, 847 (C-C), 1015 (C-C), 1111 (CN), 1302 (CH_2), 1357 (CH), 1413 (C-N), 1459 (CH and CH_3) cm^{-1} for alanine at low frequency regions and 2884 (CH), 2958 (CH_3), 2995 (CH_2), and 3084 (C-H stretching mode) at high frequency regions.[19-20] The molecular structure of glutamine is $C_5H_{10}N_2O_3$ and sharp peaks are detected at 110 (lattice vibration), 211 (skeletal stretch), 455 (skeletal stretch), 624 (C=O bending vibration), 852 (C-C), 1098 (NH_2 rocking vibration), 1327 (CH_2 wagging mode), 1417 (CH_2 scissoring mode), 1496 (NH_3 bending vibration), 1605 (NH_3^+), 1685 (C=O stretching mode) cm-1 for glutamine at low frequency regions and 2931, 2958, 2989, 3064, 3177, 3313, and 3404 cm^{-1} are due to CH_2 and CH stretching vibrations at high frequency.[3,20-22] In addition, the molecular structure of phenylalanine is $C_9H_{11}NO_2$ and Raman peaks at 136, 213, 320, 468 (C-C-C-C), 620, 831 (CC skeletal stretch), 1004 (deformation ring), 1034 (deformation ring), 1215 (C-H), 1312, 1449 (CH/CH_3 deformation), 1603 (C=O), and 1759 cm^{-1} for phenylalanine at low frequency regions and 2925, 2968, 3064, 3249, and 3465 cm^{-1} are due to CH stretching at high frequency regions.[23-24] These amino acids detected from a lander/rover platform will provide evidence of past or present life on Mars, Europa, and other solar bodies.

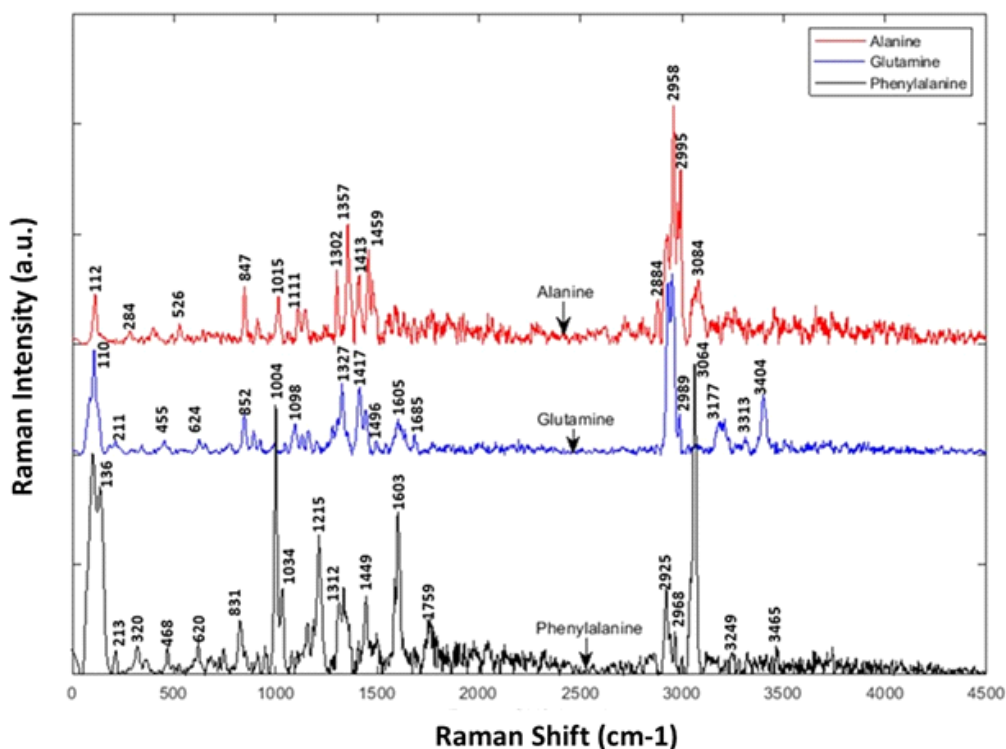Fig. 7. Sharp Raman peaks at low frequency (80 cm^{-1} – 2200 cm^{-1}) and high frequency (2500 cm^{-1} - 4500 cm^{-1}) regions of L-Alanine, L-Glutamine, and L-Phenylalanine obtained using a 532 nm pulsed laser with a line shaped laser beam (10 µm width by 5 mm height) at a distance of 6 cm.

In this article, we discuss results obtained using the SUCR system as an imaging system and Fig. 8 shows the 5 mm x 5 mm scan area with 50 µm step resolution and total steps 101. In this study, 532 nm laser as Raman line scanner creates 2-D profiles and this line scan contains a single column of pixels of ICCD camera 2 (2048 x 512 pixel format) used to capture data very quickly from the target samples. We scanned multi-layered samples consisting of glutamine, naphthalene, and sulfur inside a frozen glass jar using the SUCR system at a 6-cm target distance. The multi-layered glass jar was mounted on the surface of the motorized scanner to scan the sample. As the laser spot moves past the 5 mm in horizontal with 50-µm step resolution, a complete image is reconstructed through software line by line. We collected raw data from the scanned area through an ICCD camera (e2v CCD: 2048 x 512) to create a map of 5 mm x 5 mm area (Fig. 8a), produce individual line profiles, e.g., sulfur, glutamine, and naphthalene, and a mixed sulfur, glutamine, and naphthalene (Fig. 8b), and a 3-D plot of materials distribution map (Fig. 8c). Figs. 8a and 8b show the Raman scan image map and line profiles of individual and mixed sulfur, glutamine, and naphthalene, respectively. Fig. 9 shows Raman spectra of ice, glutamine powder, and glutamine in ice at high frequency region. The Raman signal of ice in Fig. 9 (red trace) is smaller in amplitude as compare to glutamine powder (black trace) and glutamine in ice (blue trace). Therefore, the Fig. 8c materials distribution clearly shows the detection of three mixed samples and Raman spectra of sulfur, glutamine, and naphthalene are easily identified, but the ice water is not seen in this figure. We believe this might be due to strong biofluorescence signal from glutamine masking the ice-water Raman band in the high frequency region. This Fig. 8c materials distribution scanned map is constructed using Matlab software. In the high frequency region, Raman signals are expected only from water, ice, organic, biogenic, and water containing minerals. Both naphthalene or PAH (organic) and

glutamine (biogenic) show signals in this region. This demonstrates the fast detection of biomarkers in various layers within a single Raman measurement allowing for faster Raman imaging.

5. CONCLUSIONS

We developed the SUCR instrument by integrating optical components from Kaiser, Semrock, and Thorlabs; e2v CCD 42-10 with intensifier camera from the Syntronics, LLC and a 532 nm pulsed laser from CrystaLaser, Inc. We tested each of the optical components and built the spectrometer in-house. We installed a laser and ICCD camera on the spectrometer and verified the system performance by operating the laser and detecting the Raman signals through the ICCD camera. We calibrated the CCD pixels by acquiring a neon light spectrum through the ICCD camera. Later, we acquired backscatter signals from different samples and analyzed them. We investigated water, water ice, naphthalene, sulfur, and mixed naphthalene/sulfur samples embedded in ice. We have investigated alabaster and hydrous mineral, gypsum, in dry and in ice, In addition, we have studied few amino acids, L-alanine, L-glutamine, and L-phenylalanine and extracted background fluorescence from those amino acids by using polynomial baseline correction. The Raman line scan spectra were examined in detail to identify the distribution of naphthalene, sulfur, and glutamine from mixed naphthalene, sulfur, and glutamine samples in ice across the glass jar. The line scans were analyzed to create an image and relative intensity distributions showing the Raman spectra of the mixed samples. We demonstrated the Raman scan image map and line profiles of individual and mixed sulfur, glutamine, and naphthalene, respectively. The materials distribution clearly shows the detection of three mixed samples and Raman spectra of sulfur, glutamine, and naphthalene are easily identified, but the ice water is not seen due to glutamine spectrum overlay on ice-water spectrum. In the high frequency region, Raman

signals are expected only from water, ice, organic, biogenic, and water containing minerals. Both naphthalene or PAH (organic) and glutamine (biogenic) show signals in this region. This instrument demonstrates the fast detection of biomarkers in various mixed samples within a single Raman measurement allowing for faster Raman imaging. In addition, this micro-Raman instrument demonstrates to characterize minerals, organics, and biogenic materials (amino acids) and this instrument has the capability to characterize biomarkers to provide evidence for past and present life on Mars, Europa, and other solar bodies.
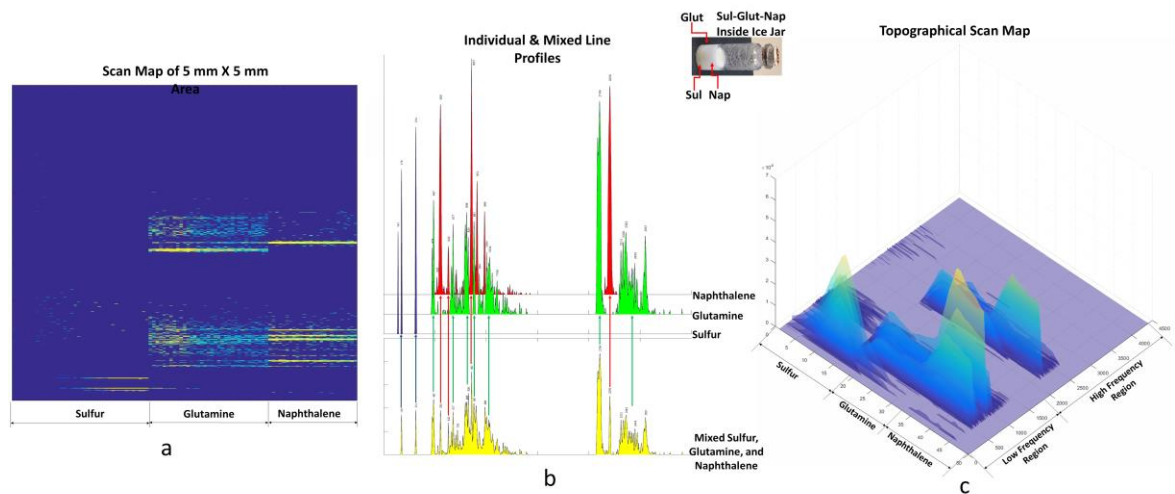

Fig. 8. Raman line scan 5 mm x 5 mm area by placing sulfur, glutamine, and naphthalene side by side inside an ice glass jar at 6-cm using ICCD camera with an E2V CCD pixel size (13.5 µm x 13.5 µm) and format 2048 x 512. a. Raman area image, b. Raman spectra of line profile (S: Sulfur, G: Glutamine, N: Naphthalene, mixed sulfur, glutamine, and naphthalene), and c. Materials Distribution.
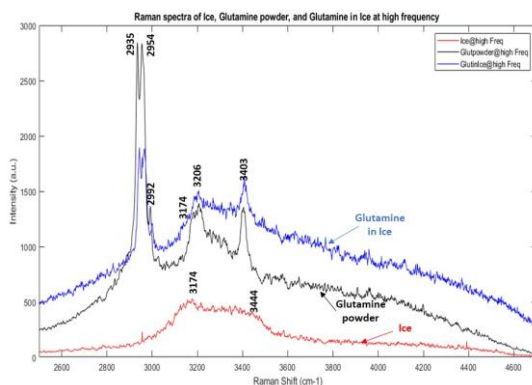

Fig. 9. Raman spectra of ice, glutamine powder, glutamine in ice.

REFERENCES

1. Visions and Voyages for Planetary Science in the Decade 2013 – 2022, National Academy Space Studies Board, March 7, 2011.
2. Europa Lander Study 2016 Report, Europa Lander Mission, JPL D 97667, Task Order NNN16D011T, Europa Lander Mission Pre-Phase A.

3. Abedin, M. N.; et al.: "Standoff ultracompact micro-Raman sensor for planetary surface explorations*." Applied Optics*, 2018. Vol. **57**(1): p. 62-68. DOI: 10.1364/ao.57.000062.

4. S. Privitera, S. Quilici, F. La Via, C. Spinella, F. Meinardi, E. Rimini,,"Kinetics of the C49–C54 transformation by micro-Raman imaging", Microelectronic Engineering 55 (2001) 109–114.

5. Dall'Asén, A. G., Sophia I. Dimas, Sarah Tyler, Jessica F. Johnston, Timothy R. Anderton, Inese I. Ivans, Jordan M. Gerton, Benjamin C. Bromley, and Scott J. Kenyon, "Mapping the composition of chondritic meteorite Northwest Africa 3118 with micro-Raman spectroscopy", SPECTROSCOPY LETTERS 2017, VOL. 50, NO. 8, 417–425.

6. L. W. Beegle, R. Bhartia, L. DeFlores, W. Abbey, B. Carrier, S. Asher, A. Burton, P. Conrad, S. Clegg, K. S. Edgett, B. Ehlmann, M. Fries, W. Hug, R. Reid, L. Kah, K. Nealson, M. Minitti, J. Popp, F. Langenhorst, V. Orphan, P. Sobron, A. Steele, N. Tarcea, G. Wanger, R. Wiens, K. Williford, R. A. Yingst,"SHERLOC: AN INVESTIGATION FOR MARS 2020", Biosignature Preservation and Detection in Mars Analog Environments (2016), Abstract #2022.

7. Misra, A. K.; et al.: "Pulsed remote Raman system for daytime measurements of mineral spectra*."Spectrochimica Acta Part A: Molecular and Biomolecular Spectroscopy*, 2005. Vol. **61**(10): p. 2281-2287.

8. Garcia, C. S.; et al.: *Remote Raman sensor system for testing of rocks and minerals*. in SPIE Homeland Security and Homeland Defense 2007. SPIE 6538.

9. Sharma, S.K.; et al.: *Compact time-resolved remote Raman system for detection of anhydrous and hydrous minerals and ices for planetary exploration.* in SPIE Space Missions and Technologies 2010. SPIE 7691.

10. Abedin, M.N.; et al.: *"Mineralogy and astrobiology detection using laser remote sensing instrument."Applied Optics*, 2015. Vol. **54**(25): p. 7598-7611.

11. Misra, A. K.; et al.: *Compact remote Raman and LIBS system for detection of minerals, water, ices, and atmospheric gases for planetary exploration*. in *SPIE Defense, Security, and Sensing*. 2011. SPIE.

12. Harvey, P.D. and I.S. Butler, "Raman spectra of orthorhombic sulfur at 40 K," J. Raman Spectrosc. 17, 329-334 (1986).

13. Garcia, C. S.; et al.: *Design and build a compact Raman sensor for identification of chemical composition*. in *SPIE Defense and Security Symposium*. 2008. SPIE 6943.

14. Sharma, S. K.; Misra, A. K.; and Lucey, P. G.: *A combined remote Raman and fluorescence spectrometer system for detecting inorganic and biological materials*. in *SPIE Asia-Pacific Remote Sensing*. Proc. of SPIE Vol. 6409, 64090K, (2006) https://doi.org/10.1117/12.693868.

15. S. D. Ross, in: V. C. Farmer (Ed), The Infrared Spectra of Minerals, Mineralogical Society, London, p 243, 1974.

16. Garcia, C.S., M.N. Abedin, S.K. Sharma, A.K. Misra, S. Ismail, S.P. Sandford, and H. Elsayed-Ali, Remote Raman sensor system for testing of rocks and minerals, Proc. Of SPIE Vol. 6538 · May 2007, pp. 65381I-1 – 65381I-9.

17. Cole, W. F. and C. J. Launcuki, "A refinement of crystal structure of gypsum CaSO4•2H2O," Acta Cryst. B30, 921, 1974.

18. Chio, C. H., S. K. Sharma, and D. W. Muenow, Raman spectroscopic studies

of gypsum between 33 and 374 K, Amer. Mineral., 89, 390, 2004.

19. Rosado, M.T.S., M.L.R.S. Duarte, and R. Fausto, "Vibrational spectra (FT-IR, Raman and MI-IR) of α- and β-alanine", Journal of Molecular Structure 410-411 (1997) 343-348.

20. Culka, A., J. Jehlicka, H.G.M. Edwards, "Acquisition of Raman spectra of amino acids using portable instruments: Outdoor measurements and comparison", Spectrochimica Acta Part A 77 (2010) 978–983

21. Dhamelincourt, P. and F. J. Ramirez, 'Polarized Micro-Raman and FT-IR Spectra of L-Glutamine', Applied Spectroscopy, Volume 47, Number 4 (1993).

22. Pawlukojc, A., K. Hołderna Natkaniec, G. Bator, I. Natkaniec, "L-glutamine: Dynamical properties investigation by means of INS, IR, RAMAN, H NMR and DFT techniques", Chemical Physics 443 (2014) 17–25

23. Freire, P.T.C., F.M. Barboza, J.A. Lima Jr., F.E.A. Melo and J.M. Filho, 'Raman Spectroscopy of Amino Acid Crystals', Chapter 10, February 2017. http://dx.doi.org/10.5772/65480.

24. Guangyong Zhu, Xian Zhu∗, Qi Fan, Xueliang Wan, "Raman spectra of amino acids and their aqueous solutions", Spectrochimica Acta Part A 78 (2011) 1187−1195.